Local Composition Activity Coefficient Model for Mixed-Gas Adsorption Equilibria

Harnoor Kaur[a], Hla Tun[a], Michael Sees, and Chau-Chyun Chen*

Department of Chemical Engineering, Texas Tech University, Lubbock, TX 79409-3121, USA

[a] Authors of equal contribution

* Corresponding author. Tel.: +1 806.834.3098. Email address: *chauchyun.chen@ttu.edu*.

Abstract

Taking into consideration the adsorbate-adsorbent interactions, a novel activity coefficient model is derived from the non-random two-liquid theory for mixed-gas adsorption equilibria. In contrast with the conventional activity coefficient models developed for bulk liquids, the new model correctly predicts negative deviations from ideality for adsorbed phase mixtures including azeotropic behavior exhibited by selected gas-adsorbent systems. Requiring a single binary interaction parameter per adsorbate-adsorbate pair, the model successfully correlates wide varieties of binary adsorption isotherm data and it should be a powerful engineering thermodynamic tool in correlating and predicting mixed-gas adsorption equilibria.

1. Introduction

The cornerstone of any gas adsorption system design lies in the accuracy of the mixed-gas adsorption equilibria predictions. The extended Langmuir isotherm equation [1, 2], useful as an empirical model to extract insight into the fundamental thermodynamics of adsorption, cannot provide predictions with sufficient accuracy for rigorous adsorption design for systems of industrial interest [3]. The Dual-site Langmuir (DSL) model, extensively investigated [4-6] for predicting binary and multicomponent gas adsorption equilibria, suffers from thermodynamic inconsistency due to the assumption of allowing the saturation capacity of each species to be different on each adsorption site [4]. Additionally, their concept of considering each binary pair to be either "perfect positive" or "perfect negative" on each site makes the extension to multicomponent system rather cumbersome. Beyond the extended Langmuir and DSL models, many theoretical models have been proposed to describe multicomponent adsorption, broadly classified as solution theories [7-10], potential theories [11-14], and statistical theories [15, 16]. However, these models often become unwieldy and difficult for practicing engineers to comprehend and use. Given their similarity to traditional vapor-liquid equilibria calculations in classical thermodynamics, solution theories are the most likely candidates for general use by practicing engineers while the other methods seem to be largely confined to academic and industrial research interests.

Myers and Prausnitz [7] used classical surface thermodynamics to develop the Ideal Adsorbed Solution Theory (IAST), which to this date is considered the benchmark for modeling mixture adsorption isotherms [17]. The authors assume the adsorbate phase behaves as an ideal solution at constant spreading pressure (π) in equilibrium with a gas phase, resulting in a Raoult's law type expression given by Eq. 1.

$$Py_i\phi_i(T,P,\boldsymbol{y}) = P_i^0(T,\pi)x_i \quad (1)$$

In Eq. 1, P is the total system pressure, y_i and x_i are the mole fractions of component i in the gas and the adsorbate phase, respectively, ϕ_i is the fugacity coefficient of component i and P_i^0 is the equilibrium gas phase pressure of pure component i at the same temperature and spreading pressure as the adsorbed mixture. The spreading pressure, π, is a surface potential analogous to the surface tension of a film on the surface and has units of energy per unit area (dynes per centimeter) [7]. The spreading pressure can be obtained using the Gibbs adsorption isotherm equation [7, 18] as follows:

$$\left(\frac{d\pi}{dlnP}\right)_T = \frac{nRT}{A} \quad (2)$$

In Eq. 2, A is the total area available for adsorption and n is the amount adsorbed at temperature T.

IAST is known to work well for chemically similar molecules of the similar size, but it fails to predict the adsorption equilibria of polar gas mixtures, such as O_2-CO and CO_2-C_3H_8 binaries, and for heterogeneous adsorbents like molecular sieves or metal organic frameworks (MOFs) [17]. Deviations from IAST behavior are typically negative, as shown by Myers and coworkers for the adsorption of mixtures on heterogeneous surfaces [4, 19]. The Real Adsorbed Solution Theory (RAST) was proposed to account for the non-ideality during adsorption [4, 20-23]. In analogy with the treatment of non-ideal solutions in vapor-liquid equilibria, the modified Raoult's law type expression in RAST can be written as Eq. 3.

$$Py_i\phi_i(T,P,\boldsymbol{y}) = P_i^0(T,\pi)x_i\gamma_i(T,\pi,\boldsymbol{x}) \quad (3)$$

In Eq. 3, γ_i is the activity coefficient of the adsorbate species i, which reflects the non-ideality of the adsorbate phase. Since the gas phase is considered ideal at the pressures of interest, ϕ_i is

taken as unity. At constant temperature and spreading pressure, Eq. 3 satisfies the Gibbs-Duhem equation [7].

In the literature, adsorbate phase activity coefficients are typically defined with two thermodynamic conditions: 1) the component activity coefficients should approach unity as the component composition approach unity, and 2) the activity coefficients of all components should approach unity as the spreading pressure approaches zero, or the limit of zero-surface coverage [21, 24]. The choice of the limit of zero-surface coverage as the reference state for the properties of adsorbed solutions is similar to choosing the ideal gas state as the reference state for the configurational properties of bulk fluids [24].

The choice of reference state for activity coefficients is a matter of convenience to describe real systems [25]. In this mixed-gas adsorption study, we choose thermodynamic condition 1) above but drop condition 2). In other words, we choose not to apply the zero-surface coverage reference state for the activity coefficients. Instead, the reference state chosen is the pure adsorbate at the same temperature and spreading pressure as the mixture. While the reference state fluid changes with the spreading pressure, the choice of the pure adsorbate reference state for the non-ideality of adsorbed solutions is similar to choosing the pure liquid state as the reference state for the configurational properties of bulk fluids in fluid phase equilibria. This treatment allows us to focus on the composition dependence of activity coefficients at constant temperature and spreading pressure without the complication of potential spreading pressure or surface coverage dependence. In doing so, the Gibbs-Duhem equation is strictly satisfied and the formulation remains thermodynamically consistent.

Various well-known activity coefficient models such as Van Laar, Wilson, NRTL, and UNIQUAC [20-23] have been used to calculate the activity coefficients of the adsorbate phase

components. However, these popular activity coefficient models were developed for bulk liquids and they do not properly account for the unique adsorbate-adsorbent interactions present in the adsorption systems. Consequently, these models are known to fail to correlate mixture isotherm data properly; the regressed model binary interaction parameters lack physical significance; the model extrapolations for multicomponent systems are not to be trusted [21, 24]. To address these issues, this study presents a novel activity coefficient expression that properly takes into consideration the effect of adsorbate-adsorbent interactions with the well-proven non-random two-liquid (NRTL) theory of Renon and Prausnitz for excess Gibbs energy functions [26, 27]. With the use of RAST, the choice of pure adsorbate at the system temperature and spreading pressure as the reference state, and the derivation of activity coefficient expression from the NRTL theory for excess Gibbs energy fucntions, the Gibbs-Duhem equation is strictly satisfied.

2. Thermodynamic Framework

2.1 New activity coefficient model

Following the NRTL theory [26], we first define the local compositions of a binary adsorbate phase. Consider the adsorption site of adsorbent "0" is surrounded by adsorbate molecule "1" and molecule "2". This can be imagined as a situation where the adsorption site connects multiple cages in a framework with molecules adsorbed in each cage, as shown in Figure 1. The local mole fractions of adsorbates around the adsorption site sum up to unity.

$$x_{10} + x_{20} = 1 \tag{4}$$

where x_{10} and x_{20} are the local mole fractions of adsorbate component 1 and adsorbate component 2, respectively. The distribution of these molecules in the local domain can be expressed in terms of bulk mole fractions, x_1 and x_2, adjusted by a Boltzmann distribution type relationship, similar to the work of Renon and Prausnitz [26].

$$\frac{x_{10}}{x_{20}} = \frac{x_1 \exp\left(-\frac{\alpha_{10} g_{10}}{RT}\right)}{x_2 \exp\left(-\frac{\alpha_{20} g_{20}}{RT}\right)} \tag{5}$$

In Eq. 5, g_{i0} is the interaction energy between the adsorbate molecule i (i = 1, 2) and the adsorption site of the adsorbent. The adsorption site is assumed not to interact energetically with its neighboring adsorption site, therefore Eq. 5 does not include any g_{00} terms. A non-randomness factor, α, related to the inverse of the coordination number [26, 27], is introduced to scale the interaction energy between the adsorbate molecules and the adsorption site on a per adsorbate molecule basis. Furthermore, the lateral adsorbate-adsorbate intermolecular interactions are assumed to be negligible compared to the adsorbate-adsorbent interactions. The local mole fractions can be obtained by combining Eqs. 4 and 5.

$$x_{10} = \frac{x_1 \exp\left(-\frac{\alpha_{10} g_{10}}{RT}\right)}{x_1 \exp\left(-\frac{\alpha_{10} g_{10}}{RT}\right) + x_2 \exp\left(-\frac{\alpha_{20} g_{20}}{RT}\right)} \tag{6}$$

$$x_{20} = \frac{x_2 \exp\left(-\frac{\alpha_{20} g_{20}}{RT}\right)}{x_1 \exp\left(-\frac{\alpha_{10} g_{10}}{RT}\right) + x_2 \exp\left(-\frac{\alpha_{20} g_{20}}{RT}\right)} \tag{7}$$

Once again following the derivation of Renon and Prausnitz [26], the molar excess Gibbs free energy of the adsorbate mixture is treated with Scott's two-liquid theory [28]. The molar excess free energy is the sum of the changes in residual Gibbs free energy involved in exchanging molecules of a pure adsorbate phase at the same temperature and spreading pressure of the adsorbate mixture with those in the solution weighted by their bulk mole fractions.

$$g^E = x_1\left(g^{(0)} - g^{(0)}_{pure,1}\right) + x_2\left(g^{(0)} - g^{(0)}_{pure,2}\right) \tag{8}$$

where $g^{(0)} = x_{10} g_{10} + x_{20} g_{20}$, $g^{(0)}_{pure,1} = g_{10}$, and $g^{(0)}_{pure,2} = g_{20}$. Eq. 8 can therefore be rewritten as Eq. 9.

$$g^E = x_1(x_{10}g_{10} + x_{20}g_{20}) + x_2(x_{10}g_{10} + x_{20}g_{20}) - x_1g_{10} - x_2g_{20} \tag{9}$$

Substituting the expressions for x_{10} and x_{20} from Eqs. 6 and 7 into Eq. 9 and assuming the non-randomness factors α_{10} and α_{20} are equivalent and constant ($\alpha_{10} = \alpha_{20} = \alpha$), the excess free energy is described by Eq. 10.

$$g^E = \frac{x_1x_2(g_{10} - g_{20})\left[\exp\left(\frac{-\alpha g_{10}}{RT}\right) - \exp\left(\frac{-\alpha g_{20}}{RT}\right)\right]}{x_1\exp\left(\frac{-\alpha g_{10}}{RT}\right) + x_2\exp\left(\frac{-\alpha g_{20}}{RT}\right)} \tag{10}$$

In keeping with the nomenclature of NRTL, Eq. 10 can be recast as Eq. 11 using the relations $\tau_{ij} = -\tau_{ji} = \frac{(g_{i0} - g_{j0})}{RT}$, and $G_{ij} = \exp(-\alpha\tau_{ij})$.

$$\frac{g^E}{RT} = \frac{x_1x_2\tau_{12}[G_{12} - 1]}{x_1G_{12} + x_2} \tag{11}$$

The activity coefficient of adsorbate component 1 in a binary mixture is related to the partial molar excess Gibbs free energy by Eq. 12.

$$RT\ln\gamma_1 = \left[\frac{\partial n_T g^E}{\partial n_1}\right]_{T,\,\pi,n_2} \tag{12}$$

Substituting Eq. 11 in Eq. 12 yields expressions for the activity coefficients of adsorbate component 1 and adsorbate component 2.

$$\ln\gamma_1 = \frac{x_2^2\tau_{12}[G_{12} - 1]}{[x_1G_{12} + x_2]^2} \tag{13}$$

$$\ln\gamma_2 = \frac{x_1^2\tau_{21}[G_{21} - 1]}{[x_1 + x_2G_{21}]^2} \tag{14}$$

Eqs. 13 and 14 represent the new activity coefficient expressions for the components in a binary mixture of the adsorbate phase, referred to as the adsorption Non-Random Two-Liquid equation (aNRTL). According to Eqs. 13 and 14, there are two adjustable parameters: α and τ_{12}. Following the NRTL model convention, the value of α is not obtained from single or binary

isotherm data but is fixed empirically at 0.2 or 0.3 [26, 27]. τ_{12} is the pair-wise binary interaction parameter to be regressed from binary isotherm data and it reflects the difference in the adsorbate-adsorbent interactions for the two adsorbates. Since g_{10} and g_{20} represent the attractive interaction energy involved in adsorption, both values are negative. If $\tau_{12} < 0$, then the g_{10} interaction is stronger (more negative) compared to g_{20}, implying that component 1 is the thermodynamically preferred adsorbate. Conversely, if $\tau_{12} > 0$, then g_{20} interaction is stronger and component 2 would be the thermodynamically preferred adsorbate. Furthermore, if $\tau_{12} \approx 0$, the adsorbent has no preference for either adsorbates, the adsorbate activity coefficients are unity, and the corresponding adsorbate phase behaves as an ideal solution described by IAST.

As mentioned earlier, we assume the competitive adsorption is solely dependent on the difference in the adsorbate-adsorbent interactions for the adsorbate 1 – adsorbate 2 pair, τ_{12}. We make no assumptions on the spreading pressure dependence nor temperature dependence, if any, of τ_{12}. In a parallel study we have performed on pure component isotherms with aNRTL model, we have found τ_{12} for pure component isotherms properly describe the adsorbent surface heterogeneity and are independent of surface coverage extent and spreading pressure. In another parallel study we have performed on isosteric heat of adsorption with aNRTL model, we have found the temperature dependence of τ_{12} to be regular solution-like, i.e., proportional to inverse of temperature.

It is worth noting that the numerator of Eq. 11, the excess Gibbs energy expression derived from the NRTL theory for a binary adsorbate mixture, is consistent in form with the excess Gibbs energy expression proposed by Siperstein and Myers [29]. Considered perhaps "the simplest form with the built-in limits required of adsorption theory," the empirical excess function of Siperstein and Myers requires up to three adjustable parameters while the proposed

aNRTL model requires only one adjustable binary interaction parameter τ_{12}. Given proper force field parameters for the adsorbate-adsorbent interaction, it should be possible to estimate τ_{12} from adsorbate phase structure parameters such as molecular sizes and potentials of mean force from molecular simulations [27].

Eq. 11 can be easily extended for multicomponent systems with '*m*' number of components. The molar excess Gibbs free energy expression and the activity coefficient expression for multicomponent systems are given as Eqs. 15 and 16 respectively.

$$\frac{g^E}{RT} = \sum_{i=1}^{m} x_i \frac{\sum_{j=1}^{m} x_j \tau_{ij}}{\sum_{k=1}^{m} x_k G_{ki}} \tag{15}$$

$$\ln \gamma_i = \sum_{j=1}^{m} \frac{x_j^2 \tau_{ij} \left[G_{ij} - 1\right]}{\left[\sum_{k=1}^{m} x_k G_{kj}\right]^2} \tag{16}$$

To predict the activity coefficients in multicomponent systems, Eq. 16 requires only the binary interaction parameters τ_{ij} determined from binary mixed-gas adsorption isotherm data.

2.2 Sensitivity analysis of the activity coefficient model

The behavior of the aNRTL activity coefficient model depends strongly on the binary interaction parameter, τ_{12}. Figure 2 illustrates the sensitivity of the calculated activity coefficients with respect to τ_{12}. Activity coefficients, γ_i, are unity when τ_{12} is set to zero. The calculated activity coefficients are all less than one and span a larger range as τ_{12} moves away from zero, or the difference between the adsorbate-adsorbent interactions increases. This observed trend of activity coefficients exhibited by the model is qualitatively consistent with that reported by Myers at constant pressure [4]. The nonrandomness factor, α, is fixed at 0.3 for the calculations shown in Figure 2. Changing the value of α will alter the calculated activity coefficients but the overall qualitative trends remain the same.

2.3 Implementing the activity coefficient model

Implementation of the aNRTL model in mixed-gas adsorption equilibria calculations involves first fitting pure component isotherm data to obtain an accurate relationship between the adsorption amount and the gas phase pressure. Once the pure component isotherms are available, the spreading pressure of each component can be calculated by integrating the Gibbs adsorption isotherm equation, Eq. 2, under the condition that the total area available for adsorption (A) is constant.

$$\pi_i(P_i^0) = \frac{RT}{A}\int_0^{P_i^0} n_i(P)\, d\ln P \tag{17}$$

The adsorption isotherm for pure component i can be expressed using various pure component isotherm equations such as Langmuir, Freundlich, Sips (Langmuir-Freundlich), Toth, etc. Given the pure adsorbate reference state for the adsorbed solutions, the choice of various pure component isotherm equations has no bearing to the tasks of correlating data of binary adsorption isotherms and predicting mixed-gas adsorption equilibria. The only requirement is that these pure component isotherm equations accurately represent pure component isotherm data for the purpose of calculating spreading pressures. In this study, either the Langmuir or Sips isotherm equations are used to represent the pure component isotherm data; the reason being both these equations have an analytical solution for spreading pressure calculations. The Langmuir isotherm equation is given by Eq. 18, while the Sips isotherm is given by Eq. 19.

$$n_i(P) = \frac{n_i^0 bP}{1+bP} \tag{18}$$

$$n_i(P) = \frac{n_i^0 (bP)^{\frac{1}{k}}}{1+(bP)^{\frac{1}{k}}} \tag{19}$$

In Eqs. 18 and 19, n_i^0 is the maximum amount adsorbed corresponding to a complete monolayer coverage in the Langmuir model, expressed in moles per kilogram of adsorbent; b is the Langmuir adsorption constant; k is a dimensionless empirical "heterogeneity" parameter [30]. Generally speaking, the Langmuir isotherm is the model of choice since it involves only two adjustable parameters. The Sips isotherm is used when the Langmuir isotherm does not adequately correlate the isotherm data.

If τ_{ij}'s are known, then the remaining calculations with the aNRTL model are straight forward. Shown in Figure 3, the calculation algorithm for a binary gas adsorption system starts with an assumed x_1 ($x_2 = 1 - x_1$), then followed by the activity coefficient calculations with Eqs. 13 and 14. Equilibrium pressure P_i^0 and spreading pressure π_i of each component are then calculated with Eqs. 3 and 17 respectively. The value for x_1 is iterated and considered converged when the equality of the component spreading pressures is satisfied. The total number of adsorbed molecules is then calculated with Eq. 20.

$$\frac{1}{n_T} = \sum_i \frac{x_i}{n_i\left(P_i^0\right)} \tag{20}$$

The procedures described in Figure 3 can be easily extended to multicomponent systems.

3. Results and Discussion

We study binary adsorption behavior on different adsorbents including activated carbon, silica gel and various types of zeolite molecular sieves. The surface of activated carbon and silica gels is nonpolar or slightly polar and their heat of adsorption is generally low [18]. Therefore, these adsorbents are typically used for adsorbing nonpolar or weakly polar organic molecules or molecules having similar size and shape characteristics. As a result, IAST tends to give satisfactory predictions for gas mixtures adsorbed on silica gel and activated carbon. Zeolites on

the other hand are highly non-ideal, polar adsorbents [18] and therefore IAST does not give accurate predictions for adsorption with zeolites.

Tables S1 to S3 of Supporting Information enlist the values of the pure component adsorption isotherm parameters regressed using pure component isotherm data available in the literature. Tables 1 to 3 present the binary interaction parameters obtained from data regression of binary mixture adsorption data available in the literature. The objective function used in the regression of the binary mixture adsorption data is to minimize the average relative deviation (ARD %) which is defined as:

$$ARD\ \% = \frac{100}{N}\sum_{j=1}^{N}\left|\frac{x_{1,j}^{calc} - x_{1,j}^{exp}}{x_{1,j}^{exp}}\right| \tag{21}$$

where x_1^{calc} and x_1^{exp} are the calculated value and the experimental value of the mole fraction of component 1 in the adsorbate phase respectively, and *N* is the total number of data points in the binary mixture adsorption data set. The ARD's have been reported for the calculations performed using the new activity coefficient model and the IAST model.

3.1 Silica Gel

Table S1 of Supporting Information presents the pure component adsorption isotherm parameters of various systems [2, 31-33] obtained using either Langmuir or Sips equation whereas Table 1 presents the binary interaction parameters regressed using the binary mixture isotherm data of the above systems. The regressed τ_{12} values are generally close to zero, suggesting relatively ideal adsorbate phase. Therefore, the aNRTL results are only slightly better than the IAST results. As an example, Figures 4(a) and 4(b) compare the experimental isotherm data and the experimental amount adsorbed [2] respectively for the CO(1)-CO_2(2) binary mixture at 373 K and 101.3 kPa with the IAST and the aNRTL results. It can be observed that, with

$\tau_{12} = 1.457$, the aNRTL model is able to capture the non-ideality of the mixture by accurately predicting the mole fraction in the adsorbate phase and the total amount adsorbed.

3.2 Activated Carbon

Table S2 of Supporting Information enlists the pure component isotherm parameters and Table 2 enlists the binary interaction parameters regressed using the pure component and mixture adsorption isotherm data [31, 32, 34] respectively. In line with the silica gel cases above, the regressed τ_{12} values are close to zero, suggesting relatively ideal adsorbate phase. Therefore, the aNRTL results are only slightly better than the IAST predictions. Figures 5(a) and 5(b) shows the model results for the adsorbate phase composition and the amount adsorbed respectively for the C_2H_6(1)-C_3H_6(2) binary mixture [34] on activated carbon at 323 K and 10 kPa. The aNRTL model results, with $\tau_{12} = 1.422$, are significantly better than the IAST results for this binary.

3.3 Zeolites

Table S3 of Supporting Information reports the pure component isotherm parameters and Table 3 reports the binary interaction parameters for various kinds of zeolites regressed using the pure component and mixture adsorption isotherm data [21, 35-40] respectively. Figures 6 to 9 compare the experimental data with the IAST and aNRTL model results for various mixtures adsorbed on the zeolites.

Figures 6(a) and 6(b) show the comparison of the experimental equilibrium data and the experimental amount adsorbed [35] respectively for the O_2(1)-N_2(2) mixture on zeolite molecular sieve (ZSM)-5A at 144 K and 101.325 kPa with the IAST and the aNRTL model results. The aNRTL results, with $\tau_{12} = 1.409$, are superior to those of the IAST results.

Figure 7(a) illustrates a comparison of the experimental equilibrium data [35, 38] for the O_2(1)-N_2(2) mixture at different temperatures and 101.325 kPa with the aNRTL model results on

zeolite 10X. The model gives excellent predictions and clearly depicts the effect of temperature on the value of τ_{12}. It can be observed from Table 3 that the value of τ_{12} decreases from 1.868 at 144 K to 0.870 at 227 K, thereby indicating that the system becomes less non-ideal with the increase in temperature. Figure 7(b) shows the phenomena of drastically changing activity coefficients with increase in temperature. The values of activity coefficients γ_1 and γ_2 can be as low as 0.2 to 0.4 at 144 K, and are in the range of 0.7 to 1 at 227 K. This explains why IAST would give poor predictions at lower temperatures as it would not be able to capture the highly negative deviations from Raoult's law. Figure 7(c) illustrates the behavior of excess spreading pressure, $\frac{\Delta\pi A}{RT}$, which could be defined as the difference between the spreading pressure of the mixture at non-ideal conditions and the spreading pressure of the mixture at ideal conditions. This difference continues to increase with the decrease in temperature which indicates that the mixture becomes more non-ideal as temperature decreases.

Figure 8 shows the adsorption phenomena of the iC_4H_{10}(1)-C_2H_4(2) binary mixture on zeolite 13X at 323 K and 137.8 kPa, a system exhibiting azeotrope behavior. Figure 8(a) shows that the Sips equation captures well the pure component isotherm data [39] for the systems at 323 K. An interesting observation is that the pure component isotherms of iC_4H_{10} and C_2H_4 cross each other at low surface coverage which leads to an azeotrope-forming behavior as would be seen in the binary experimental data. This cross-over suggests that before the isotherms intersect, iC_4H_{10} adsorption is dominating, however C_2H_4 adsorption dominates after the intersection point. Figures 8(b) and 8(c) compare the experimental composition and the amount adsorbed [39] for the iC_4H_{10}(1)-C_2H_4(2) system with the IAST and aNRTL model results on zeolite 13X at 323 K and 137.8 kPa. IAST fails to capture the azeotrope behavior whereas the aNRTL model, with $\tau_{12} = 2.084$, quantitatively captures the binary experimental data. Although not shown, the

azeotrope disappears at the higher temperature of 373 K and the aNRTL model, with $\tau_{12} = 0.465$, accurately represents the high temperature experimental data.

3.4 Multicomponent Mixture

The new activity coefficient model is readily extendable to predict multicomponent adsorptions using the binary interaction parameters regressed from the binary mixture adsorption data. Figure 9 shows the adsorbate phase composition predictions of the ternary system C_2H_4(1)-C_3H_8(2)-CO_2(3) at 293 K and 53.3 kPa on zeolite 13X using the binary interaction parameters for the three binaries C_2H_4(1)-C_3H_8(2), C_2H_4(1)-CO_2(2) and C_3H_8(1)-CO_2(2) [40] reported in Table 3. Figure 9 shows the comparison between IAST and aNRTL predictions at fixed vapor phase compositions of C_2H_4 and C_3H_8. It is observed that, for the four experimental data points available, the aNRTL predictions match well whereas the IAST predictions deviate much from the experimental results. This is because the C_3H_8(1)-CO_2(2) binary forms an azeotrope and the IAST model fails to predict this behavior. In the contrary, Figure 9 shows that the activity coefficient model correctly predicts a slight curvature at various gas phase compositions, indicative of the non-ideal behavior of the ternary system.

4. Conclusion

We present a novel activity coefficient model for mixed-gas adsorption equilibria. The model accurately correlates binary mixture adsorption isotherm data for wide varieties of adsorbents including silica gel, activated carbon, and zeolites. To the best of our knowledge, this model is the first and only thermodynamically consistent activity coefficient model that is capable of fully representing the non-ideality of gas adsorption systems including those exhibiting azeotrope behaviors. Requiring only a single binary interaction parameter per adsorbate-adsorbate binary, the model should be a very powerful engineering thermodynamic

tool to correlate and predict mixed-gas adsorption equilibria in support of rigorous process modeling and simulation of multicomponent adsorption systems and processes. While this study focuses on the model formulation and its capability to correlate binary adsorption isotherm data, future studies will report application of the model to correlate pure component isotherms, estimation of the binary interaction parameters from pure component isotherms, estimation of isosteric heat of adsorption, and development of methodology to predict the binary interaction parameters from molecular simulations.

Acknowledgments

This material is based upon work supported by the U.S. Department of Energy's Office of Energy Efficiency and Renewable Energy (EERE) under the Advanced Manufacturing Office Award Number DE-EE0007888. The authors further acknowledge the financial support of the Jack Maddox Distinguished Engineering Chair Professorship in Sustainable Energy, sponsored by the J.F Maddox Foundation.

References

[1] I. Langmuir, "The adsorption of gases on plane surfaces of glass, mica and platinum," *Journal of the American Chemical society,* vol. 40, no. 9, pp. 1361-1403, 1918.

[2] E. C. Markham and A. F. Benton, "The adsorption of gas mixtures by silica," *Journal of the American Chemical Society,* vol. 53, no. 2, pp. 497-507, 1931.

[3] S. Bartholdy, M. G. Bjørner, E. Solbraa, A. Shapiro, and G. M. Kontogeorgis, "Capabilities and limitations of predictive engineering theories for multicomponent adsorption," *Industrial & Engineering Chemistry Research,* vol. 52, no. 33, pp. 11552-11563, 2013.

[4] A. L. Myers, "Activity coefficients of mixtures adsorbed on heterogeneous surfaces," *AIChE Journal,* vol. 29, no. 4, pp. 691-693, 1983.

[5] P. M. Mathias *et al.*, "Correlation of multicomponent gas adsorption by the dual-site Langmuir model. Application to nitrogen/oxygen adsorption on 5A-zeolite," *Industrial & Engineering Chemistry Research,* vol. 35, no. 7, pp. 2477-2483, 1996.

[6] J. A. Ritter, S. J. Bhadra, and A. D. Ebner, "On the use of the dual-process Langmuir model for correlating unary equilibria and predicting mixed-gas adsorption equilibria," *Langmuir,* vol. 27, no. 8, pp. 4700-4712, 2011.

[7] A. L. Myers and J. M. Prausnitz, "Thermodynamics of mixed-gas adsorption," *AIChE Journal,* vol. 11, no. 1, pp. 121-127, 1965.

[8] S. Sircar and A. L. Myers, "Surface potential theory of multilayer adsorption from gas mixtures," *Chemical Engineering Science,* vol. 28, no. 2, pp. 489-499, 1973.

[9] M. Sakuth, J. Meyer, and J. Gmehling, "Measurement and prediction of binary adsorption equilibria of vapors on dealuminated Y-zeolites (DAY)," *Chemical Engineering and Processing: Process Intensification,* vol. 37, no. 4, pp. 267-277, 1998.

[10] S. Suwanayuen and R. P. Danner, "Vacancy solution theory of adsorption from gas mixtures," *AIChE Journal,* vol. 26, no. 1, pp. 76-83, 1980.

[11] M. Polanyi, "Adsorption von Gasen (Dampfen) durch ein festes nichtfluchtiges Adsorbens," *Verhandlungen der Deutschen Physekalischen Gesellschaft,* vol. 18, pp. 55-80, 1916.

[12] M. M. I. Dubinin, "Physical adsorption of gases and vapors in micropores," in *Progress in Surface and Membrane Science*, vol. 9: Elsevier, 1975, pp. 1-70.

[13] M. M. Dubinin, "Fundamentals of the theory of adsorption in micropores of carbon adsorbents: characteristics of their adsorption properties and microporous structures," *Pure and Applied Chemistry,* vol. 61, no. 11, pp. 1841-1843, 1989.

[14] A. A. Shapiro and E. H. Stenby, "Potential theory of multicomponent adsorption," *Journal of Colloid and Interface Science,* vol. 201, no. 2, pp. 146-157, 1998.

[15] D. M. Ruthven, "Simple theoretical adsorption isotherm for zeolites," *Nature Physical Science,* vol. 232, no. 29, p. 70, 1971.

[16] A. Martinez, M. Castro, C. McCabe, and A. Gil-Villegas, "Predicting adsorption isotherms using a two-dimensional statistical associating fluid theory," *The Journal of Chemical Physics,* vol. 126, no. 7, p. 074707, 2007.

[17] K. S. Walton and D. S. Sholl, "Predicting multicomponent adsorption: 50 years of the ideal adsorbed solution theory," *AIChE Journal,* vol. 61, no. 9, pp. 2757-2762, 2015.

[18] R. T. Yang, *Gas separation by adsorption processes*. Stoneham, MA: Butterworth-Heinemann, 2013.

[19] J. Dunne and A. L. Myers, "Adsorption of gas mixtures in micropores: effect of difference in size of adsorbate molecules," *Chemical Engineering Science,* vol. 49, no. 17, pp. 2941-2951, 1994.

[20] E. Costa, J. L. Sotelo, G. Calleja, and C. Marron, "Adsorption of binary and ternary hydrocarbon gas mixtures on activated carbon: experimental determination and theoretical prediction of the ternary equilibrium data," *AIChE Journal,* vol. 27, no. 1, pp. 5-12, 1981.
[21] O. Talu and I. Zwiebel, "Multicomponent adsorption equilibria of nonideal mixtures," *AIChE Journal,* vol. 32, no. 8, pp. 1263-1276, 1986.
[22] S. Sochard, N. Fernandes, and J. M. Reneaume, "Modeling of adsorption isotherm of a binary mixture with real adsorbed solution theory and nonrandom two-liquid model," *AIChE Journal,* vol. 56, no. 12, pp. 3109-3119, 2010.
[23] D. G. Steffan and A. Akgerman, "Thermodynamic modeling of binary and ternary adsorption on silica gel," *AIChE Journal,* vol. 47, no. 5, pp. 1234-1246, 2001.
[24] O. Talu, J. Li, and A. L. Myers, "Activity coefficients of adsorbed mixtures," *Adsorption,* vol. 1, no. 2, pp. 103-112, 1995.
[25] J. M. Prausnitz, R. N. Lichtenthaler, and E. G. de Azevedo, *Molecular thermodynamics of fluid-phase equilibria*. Upper Saddle River, New Jersey: Pearson Education, 1998.
[26] H. Renon and J. M. Prausnitz, "Local compositions in thermodynamic excess functions for liquid mixtures," *AIChE Journal,* vol. 14, no. 1, pp. 135-144, 1968.
[27] A. Ravichandran, R. Khare, and C. C. Chen, "Predicting NRTL binary interaction parameters from molecular simulations," *AIChE Journal,* vol. 64, no. 7, pp. 2758-2769, 2018.
[28] R. L. Scott, "Corresponding states treatment of nonelectrolyte solutions," *The Journal of Chemical Physics,* vol. 25, no. 2, pp. 193-205, 1956.
[29] F. R. Siperstein and A. L. Myers, "Mixed-gas adsorption," *AIChE Journal,* vol. 47, no. 5, pp. 1141-1159, 2001.
[30] D. D. Do, *Adsorption analysis: equilibria and kinetics*. London: Imperial College Press London, 1998.
[31] W. K. Lewis, E. R. Gilliland, B. Chertow, and W. H. Hoffman, "Vapor—adsorbate[1] equilibrium. I. propane—propylene on activated carbon and on silica gel," *Journal of the American Chemical Society,* vol. 72, no. 3, pp. 1153-1157, 1950.
[32] W. K. Lewis, E. R. Gilliland, B. Chertow, and W. Milliken, "Vapor—adsorbate equilibrium. II. acetylene—ethylene on activated carbon and on silica gel," *Journal of the American Chemical Society,* vol. 72, no. 3, pp. 1157-1159, 1950.
[33] W. K. Lewis, E. R. Gilliland, B. Chertow, and D. Bareis, "Vapor—adsorbate equilibrium. III. the effect of temperature on the binary systems ethylene—propane, ethylene—propylene over silica gel," *Journal of the American Chemical Society,* vol. 72, no. 3, pp. 1160-1163, 1950.
[34] E. Costa, G. Calleja, C. Marron, A. Jimenez, and J. Pau, "Equilibrium adsorption of methane, ethane, ethylene, and propylene and their mixtures on activated carbon," *Journal of Chemical and Engineering Data,* vol. 34, no. 2, pp. 156-160, 1989.
[35] R. P. Danner and L. A. Wenzel, "Adsorption of carbon monoxide-nitrogen, carbon monoxide-oxygen, and oxygen-nitrogen mixtures on synthetic zeolites," *AIChE Journal,* vol. 15, no. 4, pp. 515-520, 1969.
[36] Y. D. Chen, J. A. Ritter, and R. T. Yang, "Nonideal adsorption from multicomponent gas mixtures at elevated pressures on a 5A molecular sieve," *Chemical Engineering Science,* vol. 45, no. 9, pp. 2877-2894, 1990.
[37] G. Calleja, J. Pau, and J. A. Calles, "Pure and multicomponent adsorption equilibrium of carbon dioxide, ethylene, and propane on ZSM-5 zeolites with different Si/Al ratios," *Journal of Chemical & Engineering Data,* vol. 43, no. 6, pp. 994-1003, 1998.
[38] J. T. Nolan, T. W. McKeehan, and R. P. Danner, "Equilibrium adsorption of oxygen, nitrogen, carbon monoxide, and their binary mixtures on molecular sieve type 10X," *Journal of Chemical and Engineering Data,* vol. 26, no. 2, pp. 112-115, 1981.

[39] S. H. Hyun and R. P. Danner, "Equilibrium adsorption of ethane, ethylene, isobutane, carbon dioxide, and their binary mixtures on 13X molecular sieves," *Journal of Chemical and Engineering Data,* vol. 27, no. 2, pp. 196-200, 1982.

[40] G. Calleja, A. Jimenez, J. Pau, L. Dominguez, and P. Perez, "Multicomponent adsorption equilibrium of ethylene, propane, propylene and CO_2 on 13X zeolite," *Gas Separation & Purification,* vol. 8, no. 4, pp. 247-256, 1994.

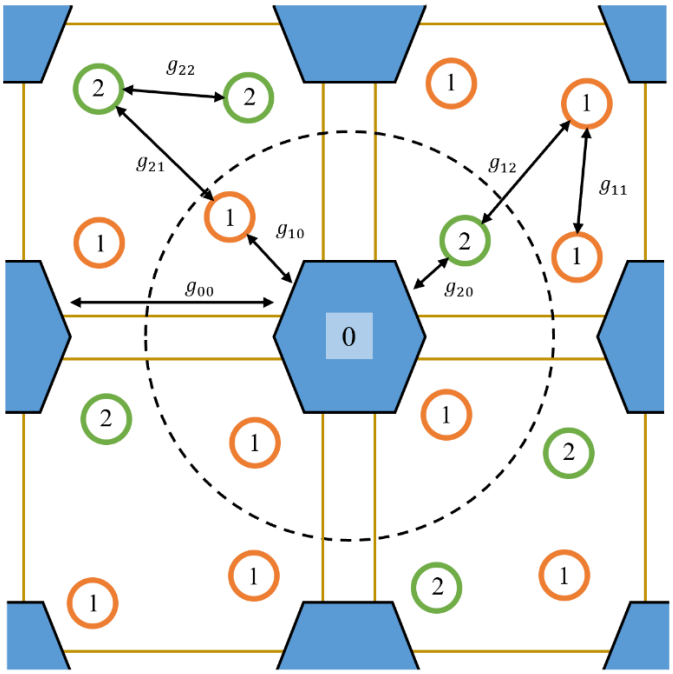

Figure 1. Schematic representation of the adsorbent cage structure and various types of pair-wise interactions

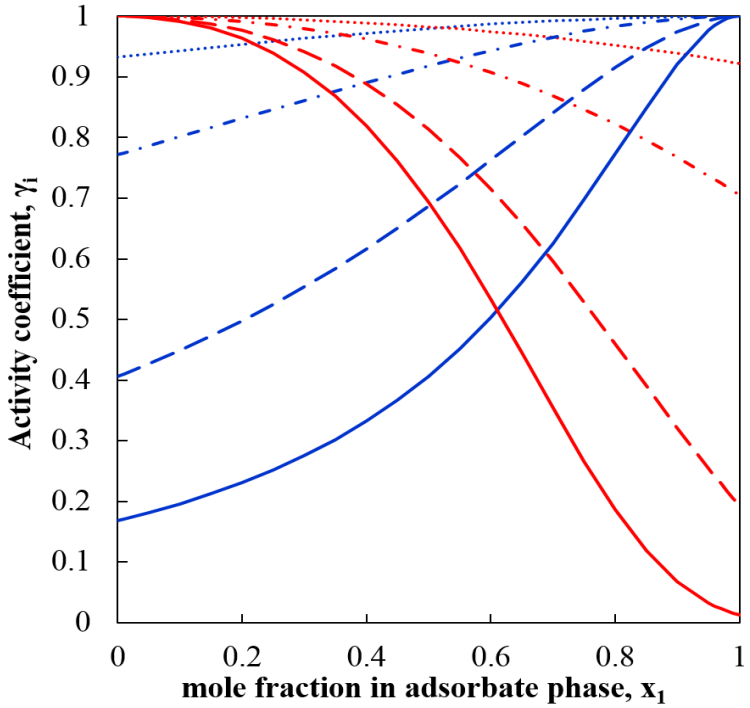

Figure 2. Sensitivity of activity coefficients, γ_1 = (——) and γ_2 = (——) with respect to different values of τ_{12} and $\alpha = 0.3$. $\tau_{12} = 0.5$ (dotted line), $\tau_{12} = 1$ (dotted dashed line), $\tau_{12} = 2$ (dashed line) and $\tau_{12} = 3$ (solid line)

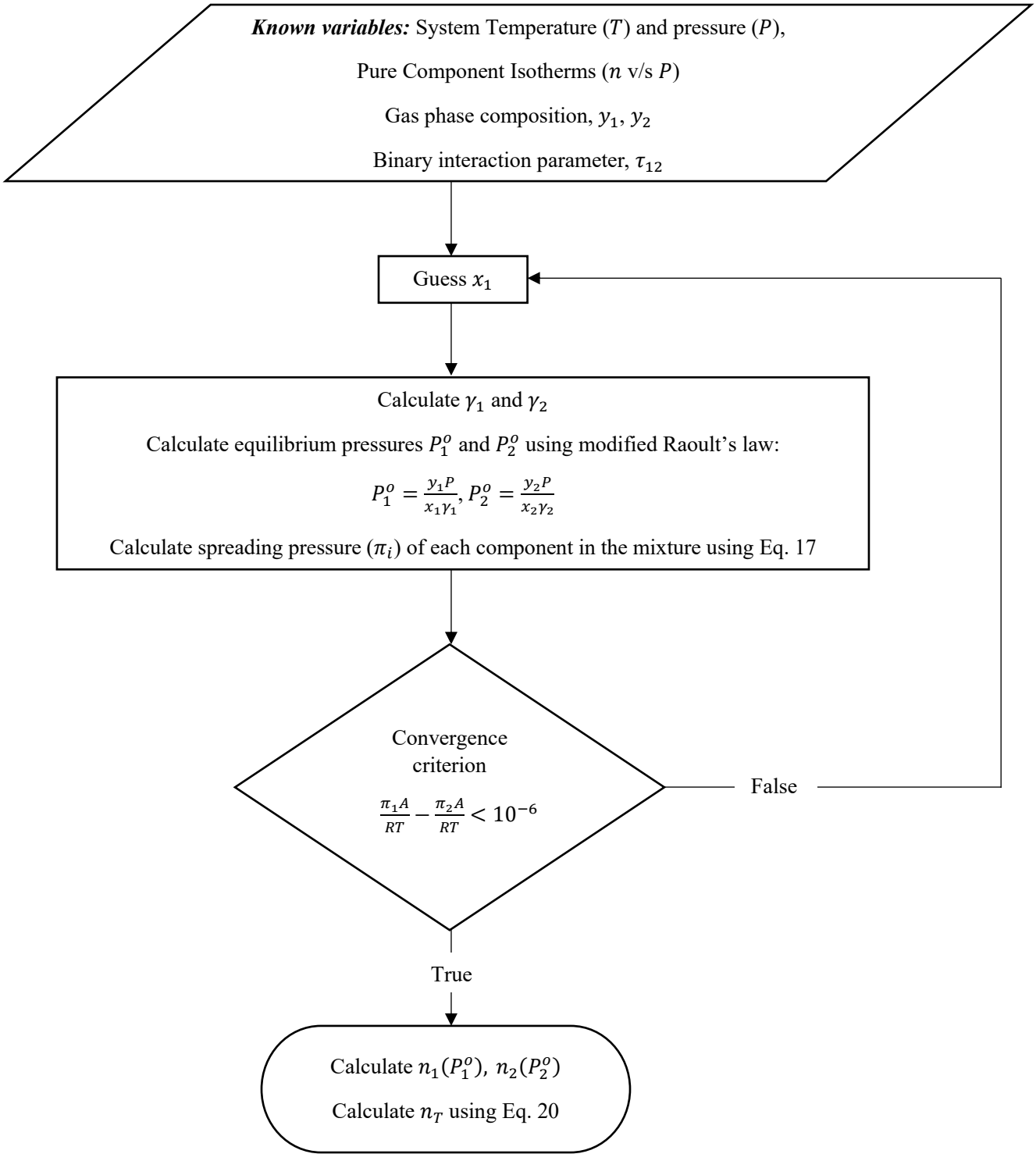

Figure 3. Algorithm for calculating adsorbate phase composition, x_i, and adsorption amount, n_T, given system temperature (T) and pressure (P), gas phase composition, y_i, and binary interaction parameter, τ_{12}

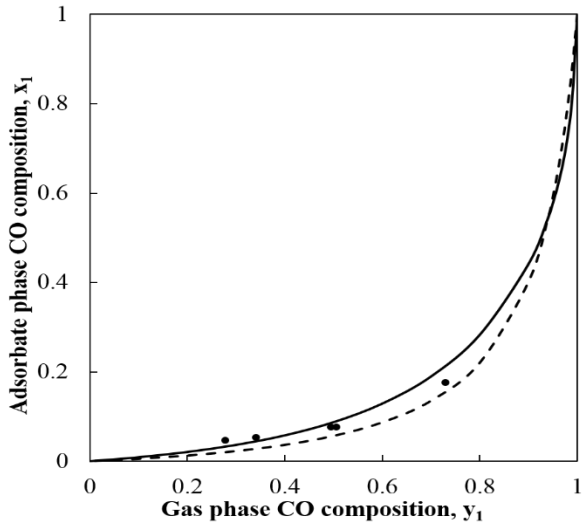

(a)

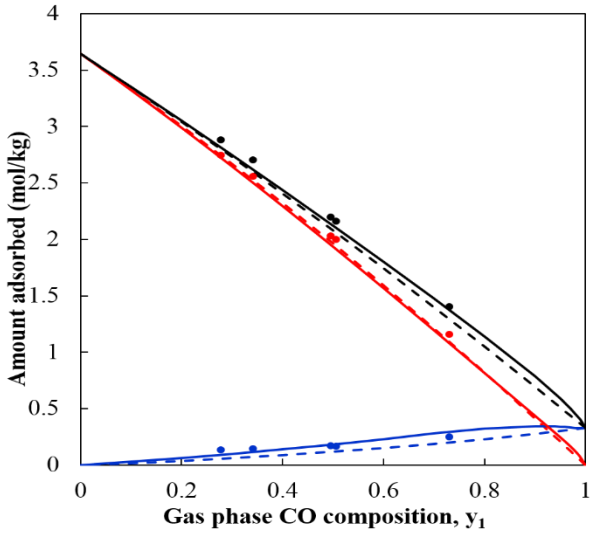

(b)

Figure 4. a) Comparison of experimental equilibrium data [2] of adsorbed CO(1, ●)-CO_2 (2) binary mixture on silica gel at 373 K and 101.325 kPa with IAST (dashed line) and aNRTL (solid line) results

b) Comparison of experimental measurement of amount adsorbed [2] for CO (1, ●), CO_2 (2, ●) and total amount of the binary mixture adsorbed (●) on silica gel at 373 K and 101.325 kPa with IAST (dashed line) and aNRTL (solid line) results

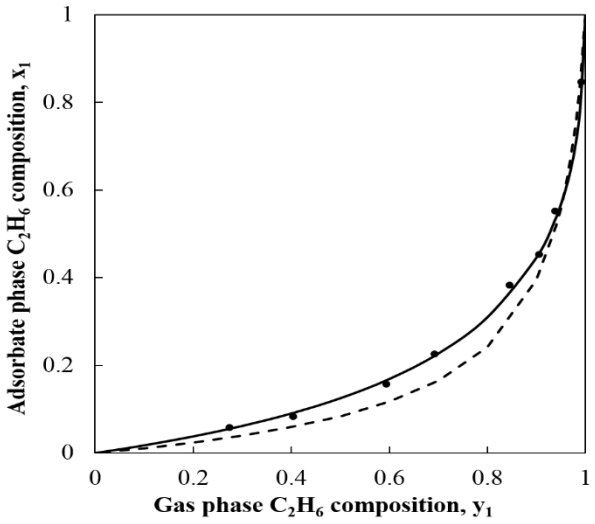

(a)

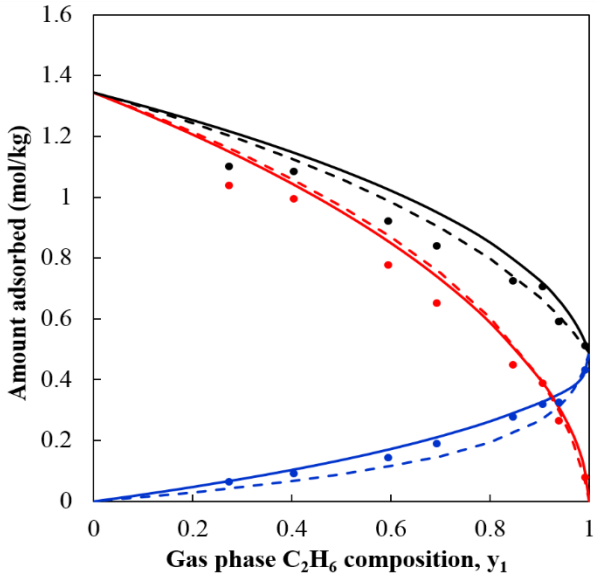

(b)

Figure 5. a) Comparison of experimental equilibrium data [34] of adsorbed C_2H_6(1, ●)-C_3H_6 (2) binary mixture on activated carbon at 323 K and 10 kPa with IAST (dashed line) and aNRTL (solid line) results

b) Comparison of experimental measurement of amount adsorbed [34] for C_2H_6 (1, ●), C_3H_6 (2, ●) and total amount of the binary mixture adsorbed (●) on activated carbon at 323 K and 10 kPa with IAST (dashed line) and aNRTL (solid line) results

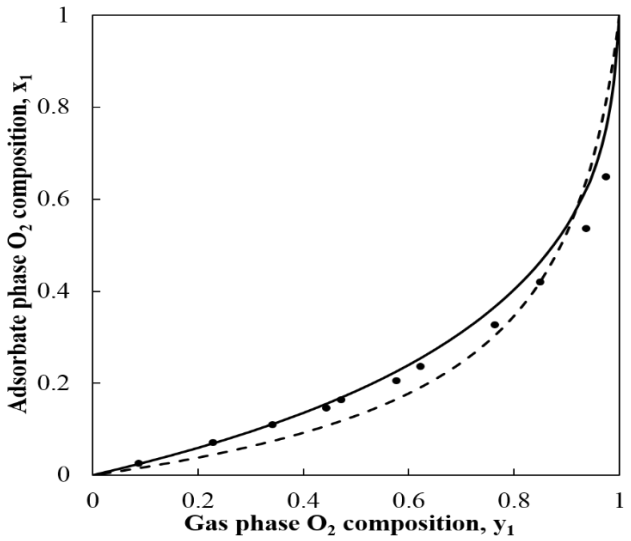

(a)

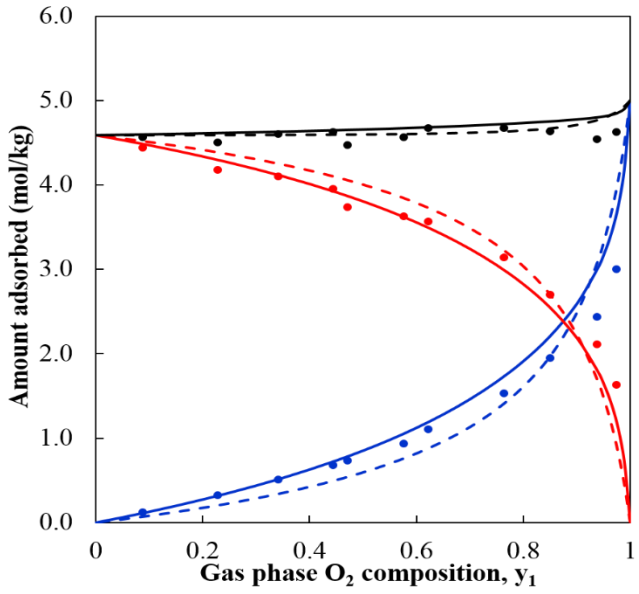

(b)

Figure 6. a) Comparison of experimental equilibrium data [35] of adsorbed O_2(1, ●)-N_2(2) binary mixture on ZSM-5A at 144 K and 101.325 kPa with IAST (dashed line) and aNRTL (solid line) results

b) Comparison of experimental measurement of amount adsorbed [35] for O_2 (1, ●), N_2 (2, ●) and total amount of the binary mixture adsorbed (●) on ZSM-5A at 144 K and 101.325 kPa with IAST (dashed line) and aNRTL (solid line) results

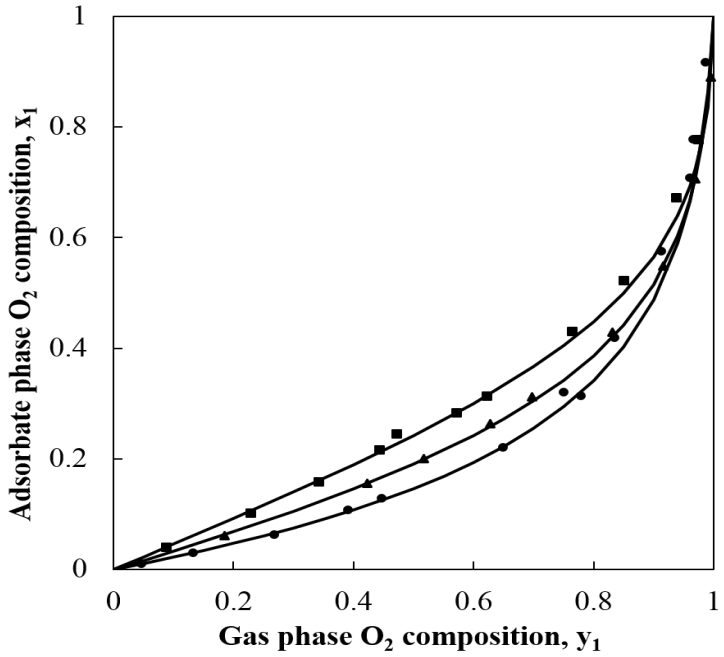
Adsorbate phase O_2 composition, x_1
Gas phase O_2 composition, y_1
0
0.2
0.4
0.6
0.8
1

(a)

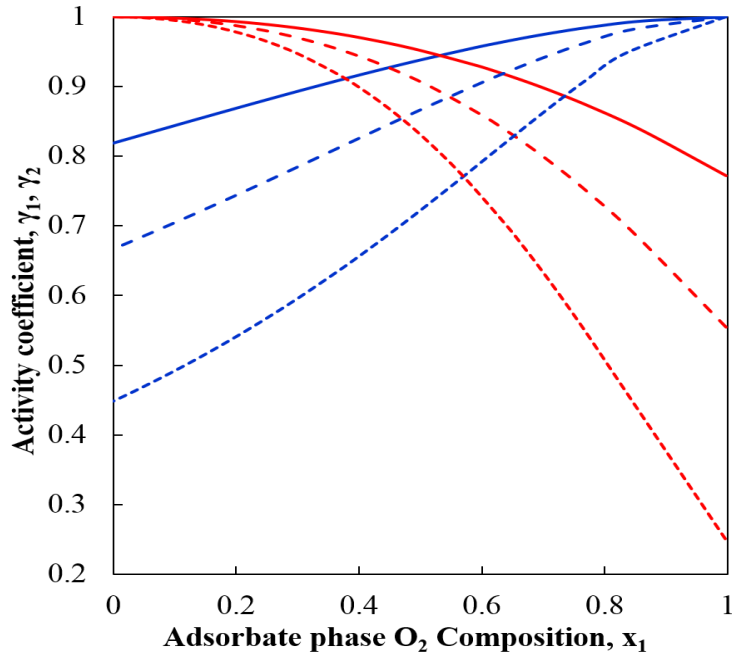
Activity coefficient, γ_1, γ_2
Adsorbate phase O_2 Composition, x_1
0.2
0.3
0.4
0.5
0.6
0.7
0.8
0.9
1
0
0.2
0.4
0.6
0.8
1

(b)

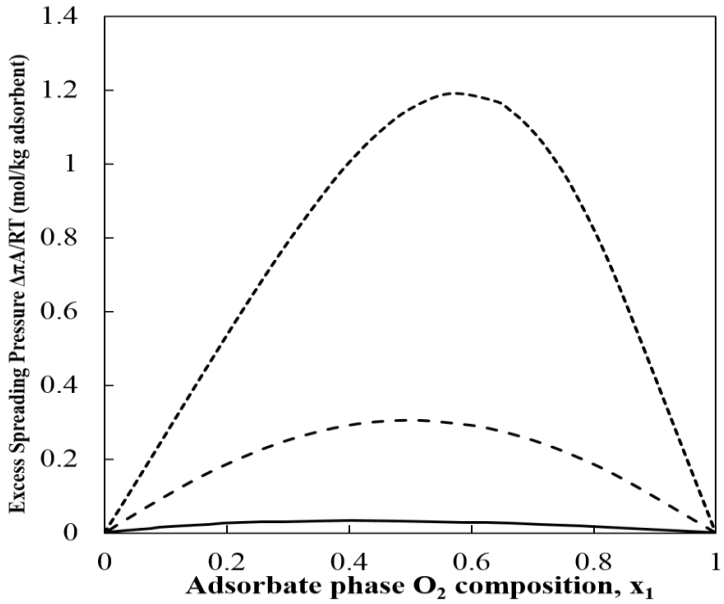

(c)

Figure 7. a) Comparison of experimental equilibrium data of adsorbed O_2(1)- N_2(2) binary mixture on zeolite 10X at 144 K (■ [35]), 172 K (▲ [39]) and 227 K (● [39]) and 101.325 kPa with IAST (dashed line) and aNRTL (solid line) results

b) Activity coefficients of adsorbed O_2(——)-N_2(——) binary mixture on zeolite 10X at 144 K (short dashed line), 172 K (dashed line) and 227 K (solid line), and 101.325 kPa

c) Excess spreading pressure of the adsorbed O_2(1)-N_2(2) binary mixture on zeolite 10X at 144 K (short dashed line), 172 K (dashed line) and 227 K (solid line), and 101.325 kPa

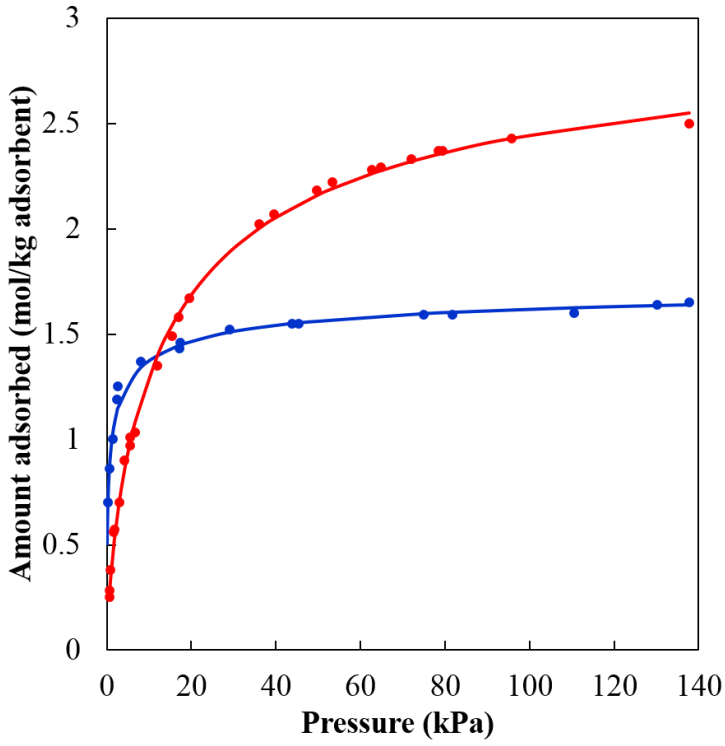
Amount adsorbed (mol/kg adsorbent)
Pressure (kPa)
0
0.5
1
1.5
2
2.5
3
0
20
40
60
80
100
120
140

(a)

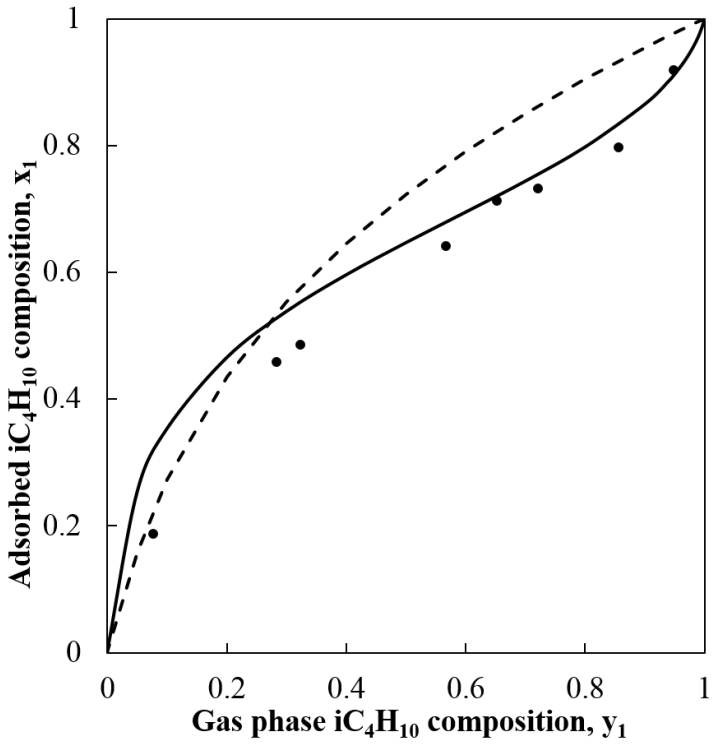
Adsorbed iC4H10 composition, x1
Gas phase iC4H10 composition, y1
0
0.2
0.4
0.6
0.8
1

(b)

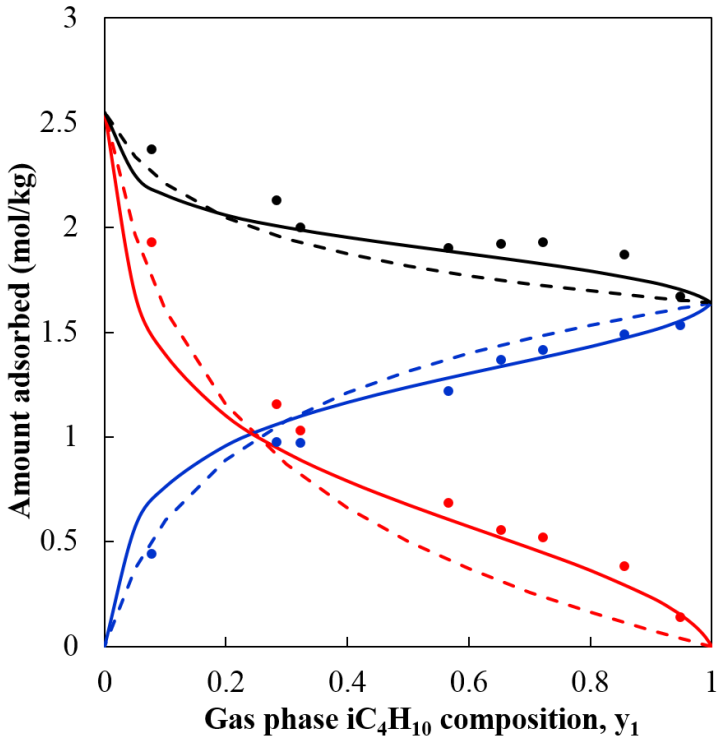

(c)

Figure 8. a) Comparison of experimental pure component adsorption isotherm data [39] of iC_4H_{10}(1, ●) and C_2H_4(2, ●) on zeolite 13X at 323 K with Sips isotherm correlations (solid line)

b) Comparison of experimental equilibrium data [39] of adsorbed iC_4H_{10}(1, ●)-C_2H_4(2) binary mixture on zeolite 13X at 323 K and 137.8 kPa with IAST (dashed line) and aNRTL (solid line) results

c) Comparison of experimental measurement of amount adsorbed [39] for iC_4H_{10} (1, ●), C_2H_4 (2, ●) and total amount of the binary mixture adsorbed (●) on zeolite 13X at 323 K and 137.8 kPa with IAST (dashed line) and aNRTL (solid line) results

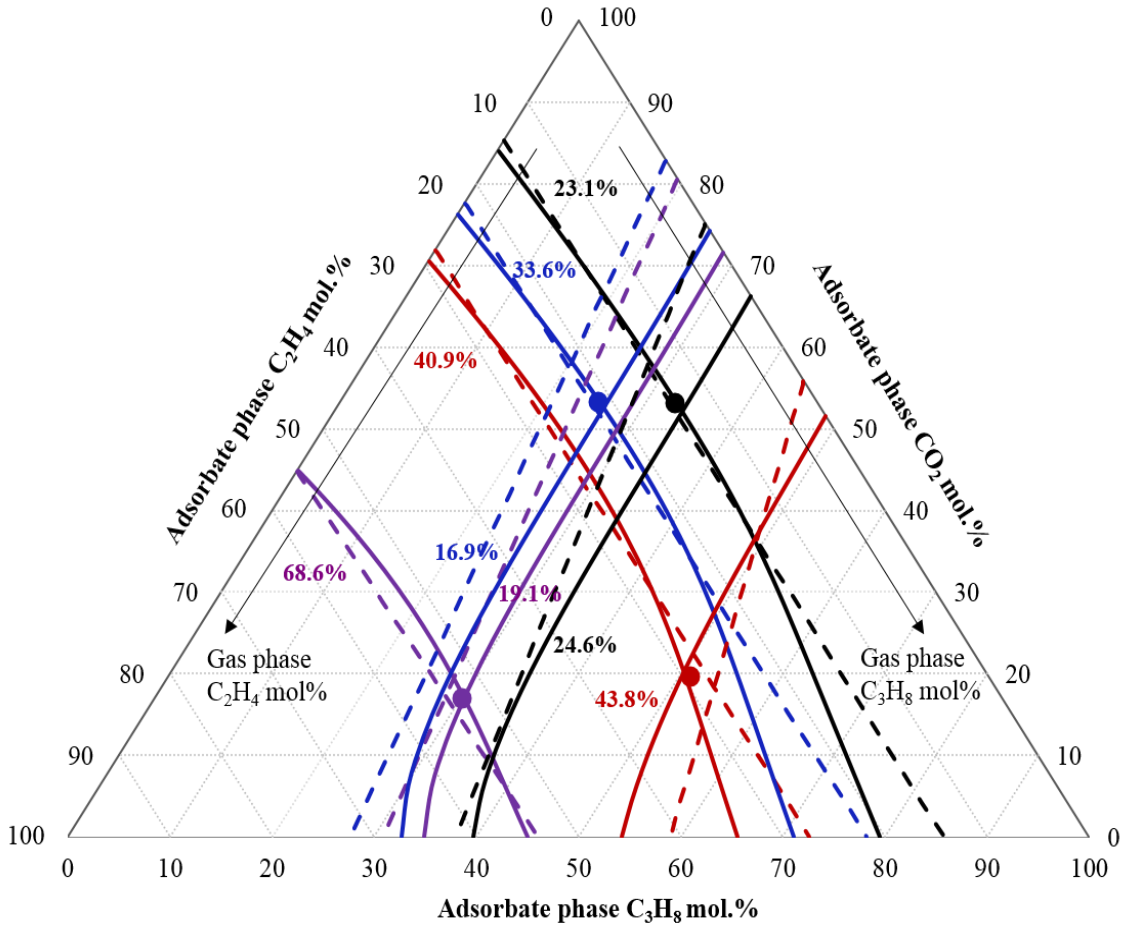

Figure 9. Prediction of adsorbate phase composition of C_2H_4(1)-C_3H_8(2)-CO_2(3) ternary system at 293 K and 53.3 kPa on zeolite 13X [40] at different vapor phase compositions of C_2H_4 and C_3H_8. The symbol (●) represents experimental data [36] of the mole percent of each species in the adsorbate phase and the (dashed line) and (solid line) represent IAST and aNRTL predictions respectively.

Table 1. Regressed values of binary interaction parameter on silica gel

Binary System	Temperature (K)	τ_{12}[a]	No. of data points	ARD % (This work)	ARD % (IAST)	Data Source
O_2(1)-CO(2)	273	0.383±0.002	3	0.97	1.84	Markhom and Benton[2]
	373	0.994±0.0005	4	0.89	6.83	
O_2(1)-CO_2(2)	373	0.912±0.002	5	17.58	18.43	
CO(1)-CO_2(2)	373	1.457±0.0005	5	17.91	33.49	
C_2H_2(1)-C_2H_4(2)	298	0	6	26.31	26.31	Lewis et al.[32]
C_3H_6(1)-C_2H_4(2)	273	-1.122±0.177	8	6.09	7.43	Lewis et al.[33]
	298	0	6	1.44	1.44	
	313	0	5	10.96	10.96	
C_3H_8(1)-C_2H_4(2)	273	-0.319±0.009	12	3.96	3.97	
	298	0	9	7.33	7.33	
	313	0	6	1.91	1.91	
C_3H_6(1)-C_3H_8(2)	298	-1.340±0.088	12 (7)	6.24	6.49	Lewis et al.[31]

[a] $\alpha = 0.3$, Numbers in the brackets represent the actual number of data points used in the regression

Table 2. Regressed values of binary interaction parameter on activated carbon

Binary System	Temperature (K)	τ_{12}	No. of data points	ARD % (This work)	ARD % (IAST)	Data Source
C_2H_2(1)-C_2H_4(2)	298	0	10	10.36	10.36	Lewis et al.[32]
C_3H_6(1)-C_3H_8(2)	298	-1.184±0.0001	18	13.53	19.03	Lewis et al.[31]
CH_4(1)-C_2H_4(2)	323	0.646±0.077	5	3.56	6.35	Costa et al.[34]
CH_4(1)-C_2H_6(2)	323	0	6	12.26	12.26	
C_2H_4(1)-C_2H_6(2)	323	0	5	5.26	5.26	
C_2H_4(1)-C_3H_6(2)	323	0.850±0.061	7	3.44	7.95	
C_2H_6(1)-C_3H_6(2)	323	1.422±0.002	8	4.68	20.50	

Table 3. Regressed values of binary interaction parameter on zeolites

Binary System	Temperature (K)	τ_{12}	No. of data points	ARD % (This work)	ARD % (IAST)	Data Source
ZSM 5A						
O_2(1)-N_2(2)	144	1.409±0.008	11	7.23	23.36	Danner and Wenzel[35]
H_2(1)-CO(2)	298	3.398±0.004	13	13.03	81.74	Chen et al. [36]
	373	2.345±0.003	12	13.43	44.41	
CO_2(1)-C_2H_4(2)	293	0.508±0.031	42	2.30	3.56	Calleja et al.[37]
CO_2(1)-C_3H_8(2)		2.223±0.009	38	6.72	38.57	
C_2H_4(1)-C_3H_8(2)		2.535±0.005	39	12.54	35.92	
Zeolite 10X						
O_2(1)-N_2(2)	144	1.868±0.003	11	3.08	30.65	Danner and Wenzel[35]
O_2(1)-N_2(2)	172	1.275±0.015	9	1.65	15.66	Nolan et al.[38]
	227	0.870±0.010	13	4.96	11.56	
O_2(1)-CO(2)	144	2.287±0.006	11	2.94	51.79	Danner and Wenzel[35]
O_2(1)-CO(2)	172	1.517±0.002	16	2.30	30.19	Nolan et al.[38]
	227	1.276±0.013	14	21.45	37.38	
Zeolite 13X						
C_2H_4(1)-CO_2(2)	298	1.863±0.072	6	15.86	26.43	Hyun and Danner[39]
iC_4H_{10}(1)-C_2H_4(2)	298	3.215±0.003	10	17.53	43.59	
	323	2.084±0.007	8	6.72	16.21	
	373	0.465±0.047	6	4.65	5.12	
iC_4H_{10}(1)-C_2H_6(2)	298	0	10	11.48	11.48	
C_2H_4(1)-C_3H_8(2)	293	1.487±0.004	28	9.49	19.29	Calleja et al.[40]
C_2H_4(1)-CO_2(2)		0.684±0.022	33	6.56	8.83	
C_3H_8(1)-CO_2(2)		1.723±0.071	31	20.21	27.29	
Zeolite H-Mordenite						
CO_2(1)-H_2S(2)	303	1.928±0.032	5	4.87	39.59	Talu and Zwiebel[21]
C_3H_8(1)-CO_2(2)		4.126±0.063	4	6.96	41.89	
H_2S(1)-C_3H_8(2)		-3.813±0.310	5	9.46	23.29	